Structural virology. Near-atomic cryo-EM structure of the helical measles virus nucleocapsid.

Irina Gutsche, Ambroise Desfosses, Grégory Effantin, Wai-Li Ling, Melina Haupt, Rob W H Ruigrok, Carsten Sachse, Guy Schoehn

STRUCTURAL VIROLOGY

Near-atomic cryo-EM structure of the helical measles virus nucleocapsid

Irina Gutsche,[1,2]* Ambroise Desfosses,[3]† Grégory Effantin,[1,2] Wai Li Ling,[4,5,6] Melina Haupt,[7] Rob W. H. Ruigrok,[1,2] Carsten Sachse,[3] Guy Schoehn[1,2,4,5,6]

Measles is a highly contagious human disease. We used cryo–electron microscopy and single particle–based helical image analysis to determine the structure of the helical nucleocapsid formed by the folded domain of the measles virus nucleoprotein encapsidating an RNA at a resolution of 4.3 angstroms. The resulting pseudoatomic model of the measles virus nucleocapsid offers important insights into the mechanism of the helical polymerization of nucleocapsids of negative-strand RNA viruses, in particular via the exchange subdomains of the nucleoprotein. The structure reveals the mode of the nucleoprotein-RNA interaction and explains why each nucleoprotein of measles virus binds six nucleotides, whereas the respiratory syncytial virus nucleoprotein binds seven. It provides a rational basis for further analysis of measles virus replication and transcription, and reveals potential targets for drug design.

Nonsegmented negative-strand RNA viruses (nsNSVs, or *Mononegavirales*) cause epidemics of serious respiratory tract illnesses [e.g., measles virus (MeV) and respiratory syncytial virus (RSV)] and outbreaks of lethal zoonotic diseases [e.g., Ebola virus and Nipah virus (NiV)]. Although preventable by vaccination, measles still remains one of the leading sources of death among young children worldwide (*1*). MeV belongs to the *Paramyxoviridae* family of *Mononegavirales*, which is further divided in two subfamilies: *Paramyxovirinae* (containing MeV and NiV) and *Pneumovirinae* (e.g., RSV).

The genome of negative-strand RNA viruses (NSVs) is enwrapped with the viral nucleoprotein N. The resulting ribonucleoprotein complex, called the nucleocapsid, protects the viral genetic information while providing a flexible helical template for viral transcription and replication by the viral RNA polymerase L, which, in the *Paramyxoviridae* and *Rhabdoviridae* families of *Mononegavirales*, is associated with the modular phosphoprotein cofactor P (*2*). As a unique structure in nucleic acid biology, the NSV nucleocapsid constitutes an attractive potential target for antiviral drugs without harmful side effects. Like all *Mononegavirales* nucleoproteins, MeV N is composed of two globular domains, the N- and C-terminal domains (NTD and CTD), which together form a stable peanut-shaped nucleoprotein core (N_{core}, residues 1 to 391 in MeV N) holding the RNA molecule in the interdomain cleft. In addition, like other *Paramyxovirinae*, MeV N features a long, intrinsically disordered tail domain (N_{tail}, residues 392 to 525) (Fig. 1A) that confers to the nucleocapsids a structural plasticity hampering their analysis at better than ~2 nm resolution (*3*, *4*).

Removal of the N_{tail} tightens the MeV nucleocapsid helix, decreasing both its diameter and pitch (*3*–*5*). Our previous cryo–electron microscopy (cryo-EM) map of the resulting N_{core}-RNA helix at 12 Å resolution (*5*) provided precise helical parameters and the domain organization of the MeV N_{core}, and a number of low- and medium-resolution EM reconstructions of other *Mononegavirales* nucleocapsids are available (*6*–*9*). However, the only atomic-resolution structural information about *Mononegavirales* nucleocapsids comes from x-ray crystallography of N-RNA rings obtained upon nonspecific encapsidation of short cellular RNAs by recombinant nucleoproteins of RSV (*7*) and of two rhabdoviruses (*10*, *11*), whereas such rings could not yet be observed for *Paramyxovirinae*. In addition, the crystal structure of the RNA-free NiV N_{core} (N^0_{core}) bound to a short N-terminal region of P (N^0_{core}-P_{50}) (*12*), has been solved recently. We therefore focused on the helical state of the MeV N_{core}-RNA nucleocapsid, so as to (i) obtain a high-resolution three-dimensional (3D) structure of the N_{core} monomer, (ii) identify the molecular determinants of helical nucleocapsid polymerization, and (iii) directly visualize the RNA inside the nucleoprotein and understand why each MeV nucleoprotein binds exactly six ribonucleotides, whereas the RSV N binds seven. Here, we report the 3D structure of recombinant MeV N_{core}-RNA nucleocapsids at 4.3 Å resolution, determined by single particle–based helical image analysis (*13*, *14*) (fig. S1). This cryo-EM map reveals the detailed domain architecture of the N_{core}, its secondary structure elements and many bulky side chains, the rationale of the nucleoprotein packing into a helix, and the mode of nucleoprotein-RNA interaction. Combined with the atomic structures of the RSV N and NiV N^0_{core}, this 3D reconstruction allows us to build a reliable pseudoatomic model of the MeV N_{core}-RNA helix.

The left-handed MeV N_{core}-RNA helix is composed of 12.34 nucleoprotein subunits per turn, with a pitch of 49.54 Å and an outer diameter of 190 Å, in good agreement with previous studies (*3*–*5*) (table S1). The RNA thread winds around the nucleoprotein bobbin, accommodated inside the cleft between the outward-pointing NTD and the inward-oriented CTD, and shielded from above by the N subunits from the successive helical turn (Fig. 1B). As in the nsNSV N-RNA rings, MeV N_{core} oligomerization is mainly mediated via the exchange subdomains called the NTD arm (residues 1 to 36) and the CTD arm (residues 373 to 391). Our 3D reconstruction shows how the NTD arm of the N_i protomer inserts into a groove in the CTD of the N_{i+1} subunit, whereas the CTD arm lies on top of the N_{CTD} of the N_{i-1} subunit, generating a repeated helical structure (Fig. 1, C to F). Unlike in the model of the RSV nucleocapsid (*15*), the N_{i-1} and N_{i+1} subunits in the MeV N_{core}-RNA helix do not interact directly.

The domain organization of the MeV N_{core} (Fig. 1D) corroborates the assumption that all nsNSV nucleoproteins share the same global fold (*2*, *16*) (fig. S2A). In particular, the CTD fold appears conserved among the *Paramyxoviridae* (MeV, NiV, RSV) (*7*, *12*). The major difference between the pneumovirus RSV and the *Paramyxovirinae* MeV and NiV is located, as predicted (*7*, *12*), at the distal tip of the NTD (residues 91 to 159 in MeV N). The local resolution of the cryo-EM map in this solvent-exposed region, known as an antigenic site of MeV N (residues 122 to 150) (*17*), seems to be the lowest, probably indicating mobility with respect to the nucleocapsid core (fig. S1D). In NiV N^0_{core}-P_{50} crystals, the RNA-free nucleoprotein is observed in an open state (*12*). The present structure of the MeV N_{core}-RNA monomer enables accurate modeling of the hinge motion between NTD and CTD, which has been proposed to be associated with the open-closed transition accompanying nucleocapsid formation (fig. S2, B and C) (*12*).

On the basis of the NiV N^0_{core}-P_{50} structure, the N-terminal domain of *Paramyxovirinae* P was assigned two simultaneous roles (*12*): (i) trapping the nucleoprotein in an open RNA-free conformation by rigidifying the CTD, and (ii) preventing its polymerization by interfering with the binding of the exchange subdomains. Indeed, although crystallization of NiV N^0_{core}-P_{50} required deletion of both the NTD and CTD arms, the first and second α helices of the helix-kink-helix peptide of P (Pα1 and Pα2) were shown to overlay with the NTD and CTD arm loops of RSV N, respectively (*12*). In MeV, the NTD arm begins with an α helix (residues 2 to 14) (Fig. 1D and fig. S2A) that fits into a hydrophobic groove formed by three conserved CTD α helices of the N_{i+1} subunit (Fig. 2A) (*12*). Specifically, four aromatic residues (Phe^{11}, Phe^{269}, Tyr^{303}, and Phe^{324}) that are conserved in *Paramyxovirinae* (*12*) seem to stack together, thereby fixing the NTD arm α helix and rigidifying the helix bundle around it (Fig. 2B). Furthermore, the NTD arm α helix of MeV N_{i-1} perfectly superimposes with Pα1 from the NiV N^0_{core}-P_{50} structure, although the latter

[1]CNRS, Unit for Virus Host-Cell Interactions, 38042 Grenoble, France. [2]Université Grenoble Alpes, Unit for Virus Host-Cell Interactions, 38042 Grenoble, France. [3]Structural and Computational Biology Unit, European Molecular Biology Laboratory, 69917 Heidelberg, Germany. [4]Université Grenoble Alpes, IBS, 38044 Grenoble, France. [5]CNRS, IBS, 38044 Grenoble, France. [6]CEA, IBS, 38044 Grenoble, France. [7]Institut Laue-Langevin, 38000 Grenoble, France.
*Corresponding author. E-mail: gutsche@embl.fr †Present address: School of Biological Sciences, University of Auckland, Auckland 1010, New Zealand.

is actually positioned upside down, and the CTD arm loop of the MeV N_{i+1} overlaps with Pα2 (Fig. 2C). Therefore, Pα1 may indeed compete with the NTD arm of the N_{i-1} protomer, and Pα2 with the CTD arm of the N_{i+1} protomer (*12*). The first α helix of P and the NTD arm α helix of MeV N appear to play similar roles: They lock the CTD and the NTD-CTD junction into a stable conformation, either open or closed depending on the presence of RNA in the interdomain cleft.

The MeV N_{core}-RNA structure explains biochemical observations (*18*, *19*) and demonstrates how and why each MeV N binds six ribonucleotides [three stacked bases facing the protein (i.e., "3-bases-in") and three stacked bases pointing

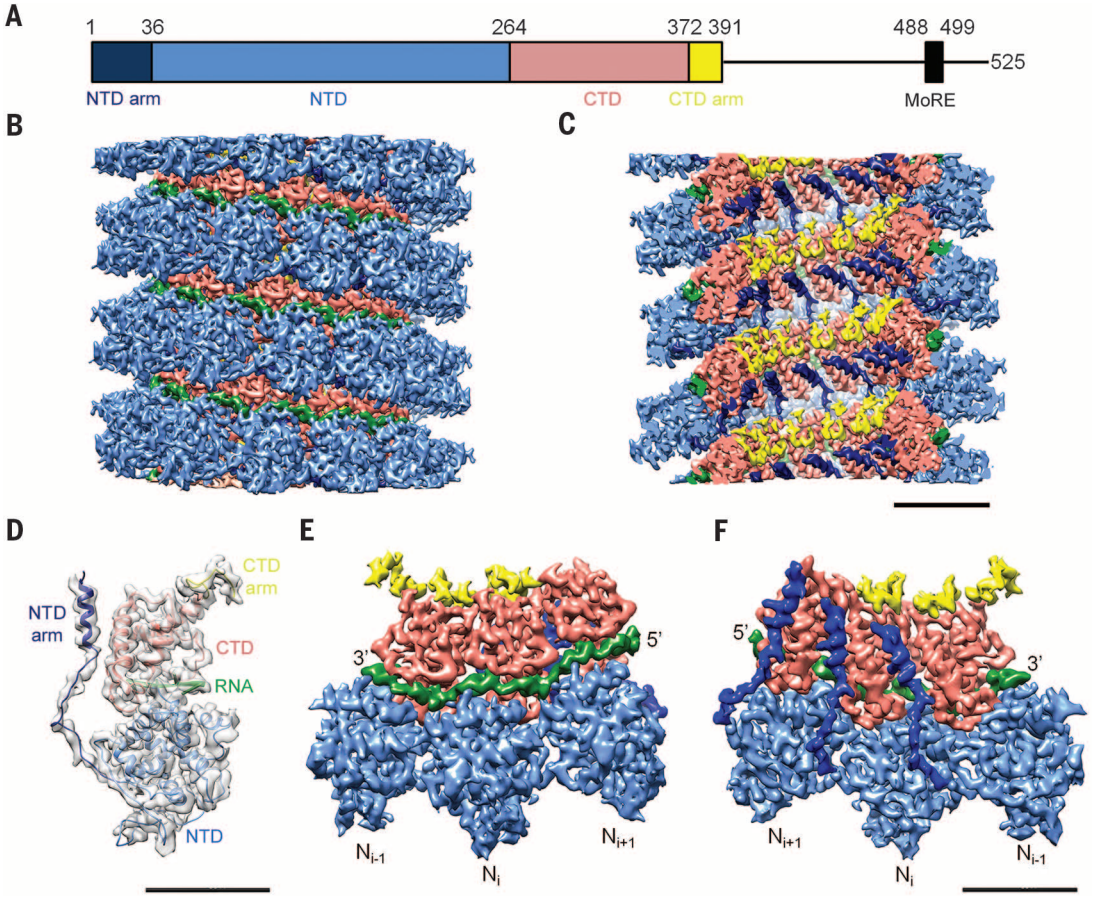

Fig. 1. Cryo-EM structure of the MeV N_{core}-RNA nucleocapsid at near-atomic resolution. (**A**) Schematic of MeV N (navy blue, NTD arm; blue, NTD; salmon, CTD; yellow, CTD arm). The same color code (with RNA in green) is used for the rest of the figure. (**B** and **C**) Isosurface representation of the cryo-EM 3D reconstruction of the helical nucleocapsid: (B) front view, (C) cutaway view. (**D**) Ribbon representation of one N_{core} monomer, with the corresponding segmented cryo-EM density shown in transparent gray. (**E** and **F**) Close-up of three consecutive protomers from the exterior (E) and from the interior (F) of the helix. Scale bars, 50 Å [(B) and (C)], 30 Å [(D) to (F)].

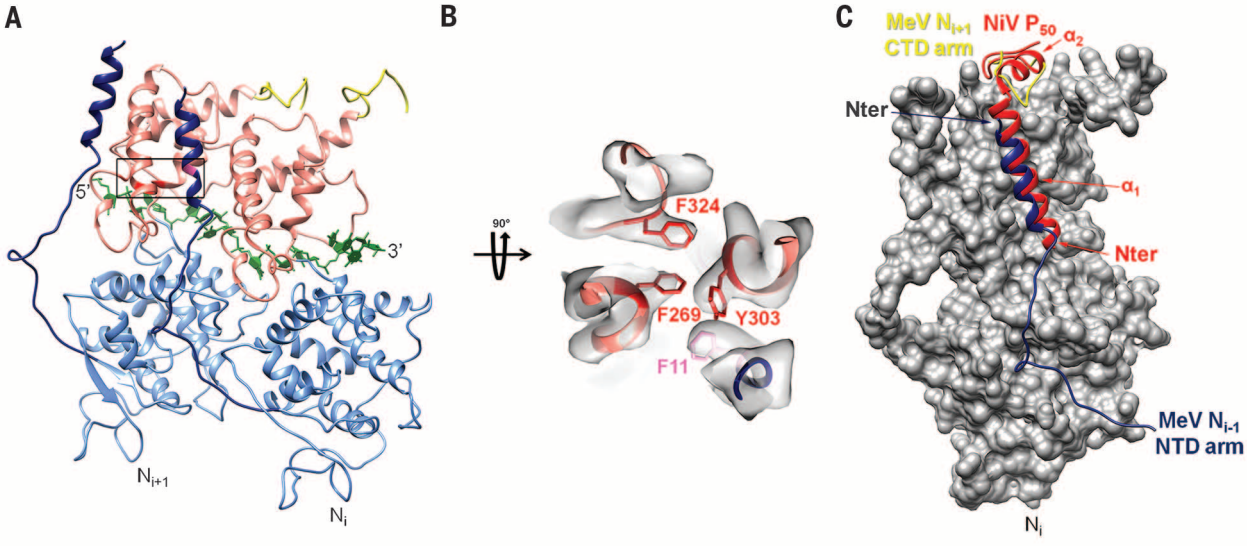

Fig. 2. Exchange domains and N_{core} oligomerization. (**A**) Ribbon representation of two consecutive protomers (colors as in Fig. 1). (**B**) Close-up of the stack of aromatics fixing the N_i subunit NTD arm on the CTD of the N_{i+1} subunit and rigidifying the CTD helix bundle. Pink, Phe^{11} of the N_i subunit; red, Phe^{269}, Tyr^{303}, and Phe^{324} of the N_{i+1} subunit; transparent gray, cryo-EM density. (**C**) The P_{50} peptide (red) of NiV superposes with the NTD arm of the MeV N_{i-1} subunit (navy blue) and the CTD arm of the N_{i+1} subunit (yellow) of MeV. The gray molecular surface represents the MeV N_i subunit. The N termini of N and P_{50} and the first and second α helices of P_{50} are indicated.

toward the solvent (i.e., "3-bases-out")], whereas RSV N binds seven ribonucleotides ("3-bases-in" and "4-bases-out") (Fig. 3, A and B, and figs. S3 and S4). In both viruses, the "3-bases-in" of the N_i subunit are 2-3-4, while base 1 stacks onto the last base of the N_{i-1} to form an outward-oriented stack of three (5-6-1) or four (5-6-7-1) bases which crosses the N_{i-1}-N_i interface, thereby probably contributing to the stability of the nucleocapsid helix. Switch 1 (between bases 1 and 2) constrains the RNA to turn inward, and switch 2 (between bases 4 and 5) orients the RNA outward again (Fig. 3, C to F, and fig. S3). Thus, the RNA topology in MeV and RSV is similar (fig. S4). In MeV nucleocapsid, the outwards-facing groove is however shorter, in particular because long conserved residues R194, K198, Q201, Q202 and Y260 (Fig. 3G) point into it from the 5′ end, sterically hindering packing of a fourth base (Fig. 3, D to F, and figs. S3 and S4). Importantly, Y260, strictly conserved in *Paramyxovirinae* and featuring a well defined side-chain cryo-EM density, does not flip away from the RNA-binding cleft upon RNA encapsidation as proposed (*12*), but stacks with base 2, orienting bases 2-3-4 "in" and therefore contributing to the switch 1 (Fig. 3, E and F). The mechanism of the switch 2 (assured by Lys^{180}, Asp^{186}, and Asn^{351} in MeV N-RNA) also differs between the two viruses (Fig. 3C and fig. S3). Finally, as in RSV, in MeV the N-RNA contacts seem to be rather RNA backbone–specific than base-specific. In particular, three positively charged residues, Lys^{180}, Arg^{194}, and Arg^{354}, show a clear side-chain density and make hydrogen bonds to the RNA backbone (Fig. 3C), and Arg^{195} (Fig. 3D) and Lys^{198} (Fig. 3E) may contribute as well. All these basic residues are conserved among *Paramyxovirinae* (Fig. 3G) and are present in equivalent positions in RSV N (*12*).

Both the nucleoprotein protomer and the entire helical nucleocapsid are dynamic entities that must rearrange during the viral replication cycle. Our findings show how the exchange subdomains of N invade the adjacent subunits in the helix, resulting in a stable and yet flexible nucleocapsid assembly. The NTD arm α helix of MeV N_i inserts into the N_{i+1} to ensure the major stabilizing interaction, whereas the CTD arm not only tethers to the N_{i-1} but also permits the intrinsically unfolded N_{tail} to escape outside between two helical turns, leading to the increased flexibility of the native MeV N-RNA (*4*, *20*). The N_{tail} appears to emerge out of the nucleocapsid core in close proximity to the RNA belt surrounding it, so as to dock the P-L complex into its functional environment on the viral genome (*21*–*23*). Thus, our structure provides a framework for understanding nucleocapsid architecture and remodeling during viral transcription and replication. It

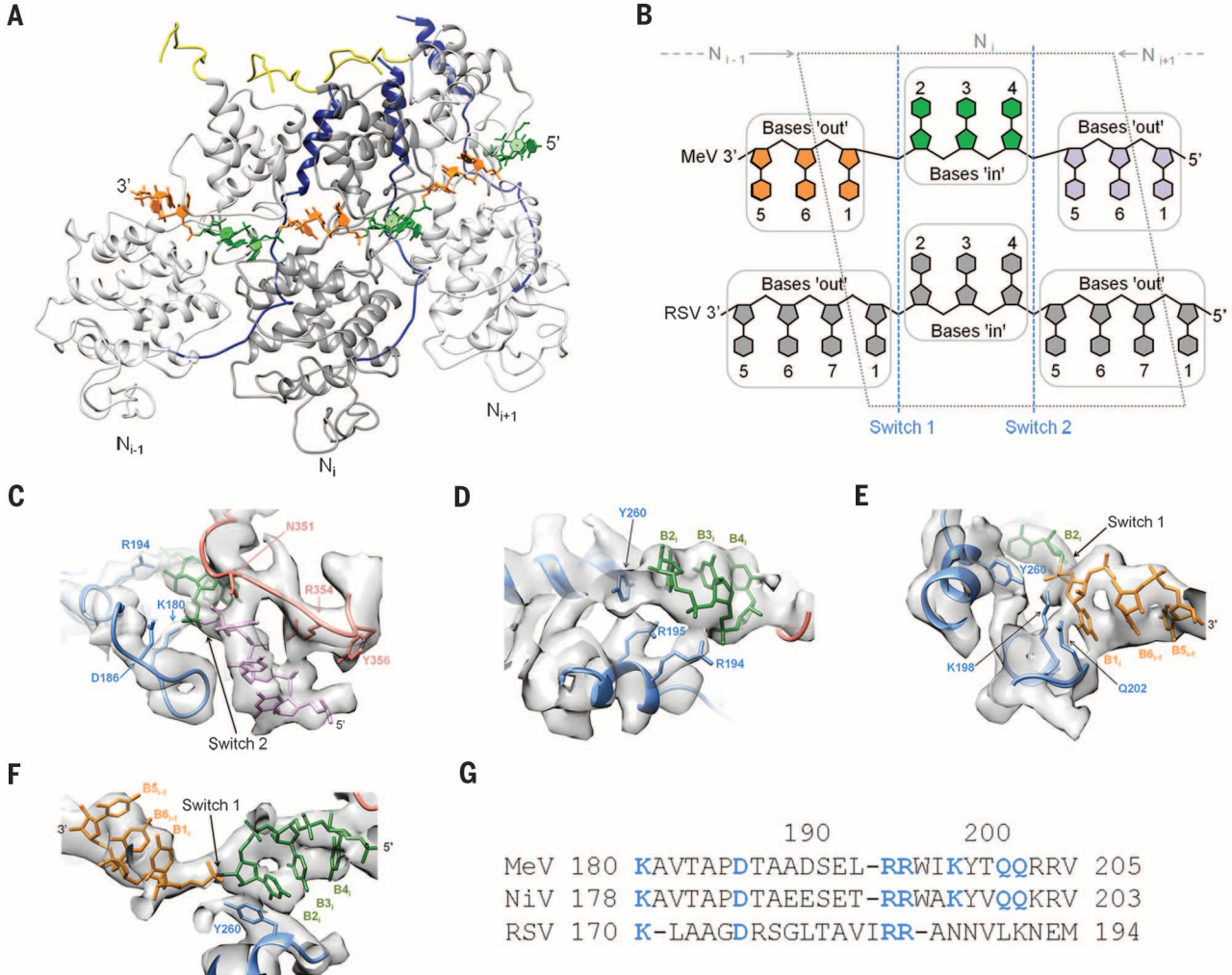

Fig. 3. Nucleoprotein-RNA interaction. (**A**) Ribbon representation of three consecutive protomers [navy blue, NTD arm; yellow, CTD arm; green, RNA (bases "in"); orange (bases "out"]. (**B**) Schematics of the RNA topology for MeV and RSV. For MeV, bases "in" are in green, bases "out" in orange and pink; RSV RNA in gray. Positions and boundaries of successive nucleoprotein subunits on the RNA are indicated; switches in RNA conformation are shown as blue dotted lines. (**C** to **F**) Close-up of protein-RNA interaction (scale bar, 10 Å). Protein colors are as in Figs. 1 and 2; RNA colors are the same as in (A) and (B). Numbers of relevant residues and bases are indicated, as are switches in RNA backbone. (**G**) Sequence alignment of the RNA-binding motif of MeV, NiV, and RSV N. Amino acid abbreviations: A, Ala; D, Asp; E, Glu; G, Gly; I, Ile; K, Lys; L, Leu; M, Met; N, Asn; P, Pro; Q, Gln; R, Arg; S, Ser; T, Thr; V, Val; W, Trp; Y, Tyr.

may also stimulate the design of new antiviral drugs, because it reveals key regions interfering with nucleoprotein oligomerization and/or genome encapsidation. Finally, because MeV shares many common features with other *Paramyxoviridae* and with nsNSVs in general, this near-atomic structure of the helical MeV N_{core}-RNA nucleocapsid may be valuable for the whole *Mononegavirales* field.

REFERENCES AND NOTES

1. www.who.int/mediacentre/factsheets/fs286/en/.
2. R. W. H. Ruigrok, T. Crépin, D. Kolakofsky, *Curr. Opin. Microbiol.* **14**, 504–510 (2011).
3. D. Bhella, A. Ralph, R. P. Yeo, *J. Mol. Biol.* **340**, 319–331 (2004).
4. A. Desfosses, G. Goret, L. Farias Estrozi, R. W. H. Ruigrok, I. Gutsche, *J. Virol.* **85**, 1391–1395 (2011).
5. G. Schoehn *et al.*, *J. Mol. Biol.* **339**, 301–312 (2004).
6. E. H. Egelman, S. S. Wu, M. Amrein, A. Portner, G. Murti, *J. Virol.* **63**, 2233–2243 (1989).
7. R. G. Tawar *et al.*, *Science* **326**, 1279–1283 (2009).
8. P. Ge *et al.*, *Science* **327**, 689–693 (2010).
9. R. Cox *et al.*, *Proc. Natl. Acad. Sci. U.S.A.* **111**, 15208–15213 (2014).
10. A. A. V. Albertini *et al.*, *Science* **313**, 360–363 (2006).
11. T. J. Green, X. Zhang, G. W. Wertz, M. Luo, *Science* **313**, 357–360 (2006).
12. F. Yabukarski *et al.*, *Nat. Struct. Mol. Biol.* **21**, 754–759 (2014).
13. A. Desfosses, R. Ciuffa, I. Gutsche, C. Sachse, *J. Struct. Biol.* **185**, 15–26 (2014).
14. See supplementary materials on *Science* Online.
15. S. E. Bakker *et al.*, *J. Gen. Virol.* **94**, 1734–1738 (2013).
16. T. J. Green *et al.*, *J. Virol.* **88**, 3766–3775 (2014).
17. R. Buckland, P. Giraudon, F. Wild, *J. Gen. Virol.* **70**, 435–441 (1989).
18. P. Calain, L. Roux, *J. Virol.* **67**, 4822–4830 (1993).
19. F. Iseni *et al.*, *RNA* **8**, 1056–1067 (2002).
20. M. R. Jensen *et al.*, *Proc. Natl. Acad. Sci. U.S.A.* **108**, 9839–9844 (2011).
21. R. L. Kingston, W. A. Baase, L. S. Gay, *J. Virol.* **78**, 8630–8640 (2004).
22. S. Longhi *et al.*, *J. Biol. Chem.* **278**, 18638–18648 (2003).
23. S. A. Krumm, M. Takeda, R. K. Plemper, *J. Biol. Chem.* **288**, 29943–29953 (2013).

ACKNOWLEDGMENTS

We thank A. Jakobi for assistance in real-space coordinate refinement using PHENIX, and M. Jamin for discussions and comments on the manuscript. This work used the platforms of the Grenoble Instruct Center (ISBG: UMS 3518 CNRS-CEA-UJF-EMBL) with support from FRISBI (ANR-10-INSB-05-02) and GRAL (ANR-10-LABX-49-01) within the Grenoble Partnership for Structural Biology (PSB); the electron microscope facility is supported by the Rhône-Alpes Region and by the Fondation pour la Recherche Medicale. A.D. received support from EMBL Interdisciplinary Postdoc (EIPOD) fellowships under Marie Curie Actions (PCOFUND-GA-2008-229597). The data reported in this manuscript are tabulated in the main paper and in the supplementary materials. The cryo-EM map of the helical MeV N_{core}-RNA nucleocapsid and the atomic model are deposited in the Electron Microscopy Data Bank and in the Protein Data Bank with accession codes EMDB-2867 and 4uft. The authors declare no competing financial interests. I.G., R.W.H.R., and G.S. designed the study; M.H. purified biological material; I.G., A.D., W.L.L., C.S., and G.S. performed research and analyzed data; R.W.H.R. and G.E. contributed to data interpretation; and I.G. wrote the paper with input from G.E.

SUPPLEMENTARY MATERIALS

www.sciencemag.org/content/348/6235/704/suppl/DC1
Materials and Methods
Figs. S1 to S4
Table S1
References (*24*–*35*)

23 December 2014; accepted 6 April 2015
Published online 16 April 2015;
10.1126/science.aaa5137

OPTOGENETICS

Engineering of a light-gated potassium channel

Cristian Cosentino,[1]* Laura Alberio,[1] Sabrina Gazzarrini,[1] Marco Aquila,[1] Edoardo Romano,[1] Solei Cermenati,[1] Paolo Zuccolini,[1] Jan Petersen,[2] Monica Beltrame,[1] James L. Van Etten,[3] John M. Christie,[2] Gerhard Thiel,[4] Anna Moroni[1]†

The present palette of opsin-based optogenetic tools lacks a light-gated potassium (K^+) channel desirable for silencing of excitable cells. Here, we describe the construction of a blue-light–induced K^+ channel 1 (BLINK1) engineered by fusing the plant LOV2-Jα photosensory module to the small viral K^+ channel Kcv. BLINK1 exhibits biophysical features of Kcv, including K^+ selectivity and high single-channel conductance, but reversibly photoactivates in blue light. Opening of BLINK1 channels hyperpolarizes the cell to the K^+ equilibrium potential. Ectopic expression of BLINK1 reversibly inhibits the escape response in light-exposed zebrafish larvae. BLINK1 therefore provides a single-component optogenetic tool that can establish prolonged, physiological hyperpolarization of cells at low light intensities.

Potassium ion (K^+) channels have a modular structure with sensor domains connected to a central ion-conducting pore (*1*). The pore integrates signals coming from the sensors and translates them into opening or closing the channel (*2*). This allows K^+ channels to alter the membrane potential of cells in response to a variety of physiological stimuli. Extending the range of signal inputs recognized by K^+ channels can be achieved by grafting exogenous sensor domains onto the pore module (*3*, *4*). With this modular interplay between sensor and pore, it is possible to engineer synthetic channels that respond to any signal by *ex novo* coupling of sensors to pores. This strategy provides new tools for the investigation and manipulation of biological functions (*5*). An attractive synthetic channel in this context is a light-gated K^+ channel, which is important because of the ability of K^+ to terminate excitatory currents within cells. This device would allow remote manipulation of the membrane potential with high temporal and spatial resolution and would represent an efficient control mechanism for many cellular processes, including neuronal firing and hormone release.

Several attempts have been made to create synthetic light-gated K^+ channels (*6*–*9*); however, these systems suffer from several shortcomings in that they require the addition of cofactors (*6*, *7*), are irreversible (*8*), or rely on multiple components (*9*). To overcome these obstacles, we engineered a single-component light-gated K^+ channel by fusing the LOV2-Jα photosensory region of a plant blue-light receptor (*10*) to the miniature K^+ channel pore Kcv (*11*). Rational design and directed evolution were employed to ultimately generate a blue-light–inducible K^+ channel that functions reversibly to drive cell membrane potentials to K^+ equilibrium in the absence of exogenous cofactors. The LOV2-Jα photoswitch from *Avena sativa* phototropin 1 (hereafter LOV) can be used to control protein activity by light-induced conformational changes (*12*). We therefore adopted this strategy to place Kcv under light control. LOV was fused to various regions of Kcv known to be mechanically important for channel gating (fig. S1A and constructs 3 to 12 in table S1).

A functional complementation approach based on the growth rescue of Δ*trk1* Δ*trk2* potassium transport–deficient yeast (strain SGY1528) (*13*) was adapted to screen for light-gated channel activity after replica plating (fig. S1B). One Kcv variant with LOV fused at the N terminus (LK) showed light-induced growth on selective agar (4 mM K^+) and liquid culture (fig. S1, B and C). LK was expressed in *Xenopus* oocytes and tested by a two-electrode voltage clamp. LK currents showed modest but reproducible increases in conductance after transfer from darkness to blue light (455 nm, 80 $\mu W/mm^2$) (fig. S2A). However, photostimulation of LK currents required tens of minutes to develop and appeared to be irreversible. In an attempt to enhance coupling of LOV to Kcv, the soluble photosensory region of LK was tethered to the plasma membrane. Introducing a putative myristoylation/palmitoylation sequence (MGCTVSAE) (*14*) at the N terminus of LK resulted in improved, but unexpected, properties. The new variant myLK (Fig. 1A and fig. S2B) showed an enhanced response to light compared with LK, but, in this case, light was found to inhibit rather than activate the channel conductance (fig. S2B). Moreover, the effect of light was reversible and it did not decrease after repetitive exposures. The light sensitivity of the channel was wavelength-specific, elicited by blue but not by red light (fig. S2B). The dynamic range of the light effect (DR), i.e., the ratio between light and dark current, was approximately 1.3. To improve the performance of myLK, three point

[1]Department of Biosciences, University of Milano, Italy. [2]Institute of Molecular, Cell and Systems Biology, University of Glasgow, UK. [3]Department of Plant Pathology and Nebraska Center for Virology, University of Nebraska-Lincoln, Lincoln, NE 68583-0900, USA. [4]Membrane Biophysics, Technical University of Darmstadt, Darmstadt, Germany.
*Present address: Illumina Italy, Via Senigallia 18/2, Milano 20161, Italy. **†Corresponding author. E-mail: anna.moroni@unimi.it**

Science

Near-atomic cryo-EM structure of the helical measles virus nucleocapsid

Irina Gutsche, Ambroise Desfosses, Grégory Effantin, Wai Li Ling, Melina Haupt, Rob W. H. Ruigrok, Carsten Sachse and Guy Schoehn

Science **348** (6235), 704-707.
DOI: 10.1126/science.aaa5137originally published online April 16, 2015

Measles virus capsid at high resolution

Viruses rely on their capsid proteins to package and protect their genome. For measles virus and other Mononegavirales family members, multiple capsid proteins together form a helical shell around the viral RNA (collectively called the nucleocapsid). Gutsche *et al.* now report a high-resolution cryoelectron microscopy structure of the measles virus nucleocapsid. The structure reveals how the nucleocapsid assembles and how the nucleo-protein and viral RNA interact, both of which may inform drug design

Science, this issue p. 704